https://doi.org/10.5194/gmd-2020-115
Preprint. Discussion started: 14 July 2020

Geoscientific Model Development Discussions
Open Access
EGU

The role of asperities in seismicity frequency-magnitude relations using the TREMOL v0.1.0. The case of the Guerrero-Oaxaca subduction zone, México

Marisol Monterrubio-Velasco[1], F. Ramón Zúñiga[2], Armando Aguilar-Meléndez[1,3], Otilio Rojas[1,4], Quetzalcóatl Rodríguez-Pérez[2,5], and Josep de la Puente[1]

[1]Barcelona Supercomputing Center - Centro Nacional de Supercomputación, Jordi Girona 29, 08034, Barcelona, Spain
[2]Universidad Nacional Autónoma de México, Centro de Geociencias, Juriquilla México
[3]Facultad de Ingeniería Civil,Universidad Veracruzana, Poza Rica, Veracruz, 93390, México
[4]Escuela de Computación, Facultad de Ciencias, Universidad Central de Venezuela, Caracas, 1040, Venezuela
[5]Consejo Nacional de Ciencia y Tecnología, Mexico City, 03940, México

Correspondence: Marisol Monterrubio-Velasco (marisol.monterrubio@bsc.es)

Abstract. Seismicity and magnitude distributions are fundamental for any type of seismic hazard analysis. The Mexican subduction zone along the Pacific Coast is one of the most active seismic zones in the world. Some peculiar characteristics of the seismicity have been observed for a subregion of the subduction regime, which has been named SUB3 in a recent seismotectonic regionalization of the country, suggesting that the observed simplicity of this source arises from the rupturing of single asperities. In this work, we numerically test this hypothesis using the TREMOL (*sThochastic Rupture Earthquake MOdeL*) v0.1.0 code. As test cases, we choose four of the most significant events ($6.5 < \mathrm{Mw} < 7.8$) that occurred in the Guerrero-Oaxaca region (SUB3) during the period 1988-2018, and whose associated seismicities are well recorded in the regional catalogs. Synthetic seismicity results show a reasonable fit to the real data, approaching it when the available data from the real events increases. These results give support to the hypothesis that single asperity ruptures mainly control seismicity in SUB3. Moreover, a fault aspect ratio sensitivity analysis is carried out to study how the synthetic seismicity varies. Our results indicate that the asperity shape is an important modeling parameter controlling the frequency-magnitude distribution of synthetic data. Therefore, TREMOL provides proper scenarios to model complex seismicity curves as that observed in the SUB3 region, highlighting its usefulness as a tool to study the earthquake process.

1 Introduction

The variation in seismicity distributions for different regions is a key input for Probabilistic Seismic Hazard Analysis (PSHA), as well as for other hazard determination approaches. The frequency-magnitude distribution on individual faults determines the specific earthquake rate of a given size at each source point, which has an important influence on the PSHA outcome

https://doi.org/10.5194/gmd-2020-115
Preprint. Discussion started: 14 July 2020

Geoscientific Model Development Discussions

(Cornell, 1968; Parsons et al., 2018). In that sense, significant efforts are oriented towards understanding, in great detail, the properties of the seismic regions as they influence the levels of seismicity. In particular, the subduction zone along the Pacific Coast of Mexico is a region where earthquakes of relevance in terms of damage (e.g. Mw $>$ 6.0) commonly take place every year (see Fig. 2). The most recent devastating cases, the 1985 M_w = 8.1 Michoacan earthquake, that killed more than 20,000 people, and the 2017 M_w = 8.2 Puebla-Morelos earthquake, which had casualties of over 98 and more than 300 injured, are two dramatic examples. As a consequence, this region is the main contributor to the seismic hazard of Mexico, although other regions also play an important role (Yazdi et al., 2019). In this context, Zúñiga et al. (2017) recently proposed a seismotectonic regionalization of Mexico with the purpose of hazard and risk assessment. Among other regions, the authors defined as SUB3 one of the subregions in the subduction regime that presents the following characteristics:

- - Seismicity in SUB3 corresponds to the shallow (h $<$ 40 km) strong coupling of subduction, covering the transitional zone of the Cocos - North American plates convergence.
- - It evolves along a plate boundary with simple and homogeneous fault surfaces, where slip takes place on single asperities (see also Singh and Mortera, 1991)
- - These features are apparent in the frequency-magnitude cumulative curve as characteristic events, which do not obey the linearity of the Gutenberg-Richter (G-R) law.

As Rodríguez-Pérez et al. (2018) pointed out, characterizing asperities at plane interfaces is important for seismic hazard analysis because they represent fault plane areas with the highest stress drops and slip values. Therefore, ruptures in these areas may generate the strongest ground motion. Ruff (1992) remarked that the distribution of the major asperities along plate boundary segments has now been determined for several subduction zones, as the Kurile Islands, Colombia, and Peru subduction zones. Also, Yamanaka and Kikuchi (2004) carried out an analysis and characterization of the asperities that produce strong earthquakes in the subduction zone in northeastern Japan. Considering the preceding observations, we present an analysis with the focus of simulating the main features that generate the seismicity at the SUB3 region. We model the SUB3 seismicity applying the *sTochastic Rupture Earthquake MOdeL* (TREMOL) (Monterrubio-Velasco et al., 2019a), that is a specialized code for the simulation of earthquake ruptures. Earlier results (Monterrubio-Velasco et al., 2019a) showed that this numerical model appropriately simulates the maximum magnitudes observed at the Mexican subduction zone. Altogether, TREMOL has also shown flexibility to simulate different scenarios with few parameters, as in the case of aftershocks following predefined faults (Monterrubio-Velasco et al., 2019b). In this work, our primary motivation is the analysis of the magnitude distribution, considering not only the largest event, but all the synthetic earthquakes generated as it pertains to the SUB3 region. In addition, we supplement our magnitude distribution analysis, by also exploring the influence of the fault aspect ratio on the synthetic seismicity. This analysis arises from observations of the relevant contribution of this fault parameter on the magnitude distribution characteristics studied in different tectonic regions (Weng and Yang, 2017; Yoder et al., 2012; Stock and Smith, 2000; Main, 2000, 1995; Main and Burton, 1989).

https://doi.org/10.5194/gmd-2020-115
Preprint. Discussion started: 14 July 2020


Geoscientific Model Development Discussions
Open Access
EGU

2 TREMOL

TREMOL is a simulation method of the earthquake rupture process that starts with the occurrence of low magnitude previous events and culminates with the mainshock. The current TREMOL implementation does not allow simulating a full earthquake cycle, because most of the tectonic load is spent during the whole process of the mainshock rupture and foreshocks, and no extra load is added during the simulation (Monterrubio-Velasco et al., 2019a). TREMOL is based on the Fiber Bundle Model (FBM) that describes the rupture process in heterogeneous materials (Hansen et al., 2015). The FBM analyzes the earthquake dynamics from the point of view of deformable materials that break under critical stresses. An implication of the FBM is the self-organized criticality behavior of the rupture process from micro to macro scale (Pradhan et al., 2010). An important TREMOL modeling parameter is the inclusion of asperities along the fault plane. As referred in the classical literature, asperities correspond to strong patches in the rupture plane that are resistive to breaking and release a larger amount of seismic moment during subsequent ruptures (Aki, 1984; Lei, 2003; Rodríguez-Pérez and Zúñiga, 2017). Among its main assumptions, TREMOL considers the existence of a main asperity in the seismic region, associated to the maximum-magnitude modeled earthquake. Even more, this asperity is assumed to have a rectangular shape with a predefined aspect ratio. Given the relevance of this single-asperity hypothesis, we define as a "Single-Asperity region", or SA region, to a rupture zone that contains a single large asperity, that experiences the largest slip during the modeled mainshock. This asperity belongs to an effective fault area, not precluding the occurrence of other previous smaller events. As mentioned above, the observed seismicity in the Mexican SUB3 subduction region can be assumed as taking place mainly at single asperity contacts, and therefore, we consider TREMOL as a suitable modeling tool to study such processes.

As described by Monterrubio-Velasco et al. (2019a), TREMOL v0.1.0 makes use of few input parameters for a complete definition of a SA region. In particular, the following three parameters are required for a general finite-fault discrete model:

1. The effective length L_{eff} $[km]$.
2. The effective width W_{eff} $[km]$.
3. The asperity size A_{a} $[km^2]$, defined for each SA region.
4. The discrete number of cells N_{cell} that defines the size of the numerical domain.

In addition, the following TREMOL parameters allow setting the load and fault strength distributions, in addition to asperity features:

4. The load conservation parameter π. After a cell fails, the TREMOL v0.1.0 algorithm transfers its load to the neighbor cells, keeping a 1-π portion of its initial load. Two parameter values of π are defined at the asperity level and at the remaining background area, named π_{asp} and π_{bkg}, respectively.
5. The asperity strength value γ_{asp}. Since, the asperity shows a physical resistance to break, this parameter allows controlling the "hardness" of the asperity, and therefore its capability to break.

https://doi.org/10.5194/gmd-2020-115
Preprint. Discussion started: 14 July 2020

Geoscientific Model Development Discussions
Open Access
EGU

6. The ratio of the asperity area $S_{\mathrm{a-Asp}}$, that is computed as,

$$S_{\mathrm{a-Asp}} = S_{\mathrm{a}} + 0.5(S_{\mathrm{a}} \cdot \alpha)\,, \tag{1}$$

where α is a random number, and $S_{\mathrm{a}} = A_{\mathrm{a}}/A_{\mathrm{eff}}$. This parameter allows setting a random size of the modeled asperity, that mimics the uncertainty and variability of real values (Somerville et al., 1999b; Murotani et al., 2008; Blaser et al., 2010; Strasser et al., 2010).

It is worth to mention that the strength γ and the load-transfer π, are our modeling devices of the physical properties of rock hardness and radiated energy, respectively.

The TREMOL workflow is summarized in three main stages. (i) A pre-processing stage where the input parameters are set. (ii) A processing stage that performs the FBM simulation of the whole rupture process. (iii) A final post-processing that converts output results into a synthetic seismic catalog. During processing, TREMOL generates numerous smaller earthquakes until the rupture of the whole asperity area $S_{\mathrm{a-Asp}}$ is achieved. In the post-processing stage, TREMOL also calculates the actual area ruptured during each earthquake, and reports such area in physical units [km^2] to allow comparisons with the whole effective area. Notice that it is possible to associate various magnitude values to the same final earthquake area, by using alternative magnitude-area relations. These magnitude values may present a strong variability with a significant impact on the synthetic seismicity curve, and then the selection of a magnitude-rupture area relation is a crucial hypothesis of this kind of studies. In this work, we use four magnitude-area relations following those proposed by Rodríguez-Pérez and Ottemöller (2013), i.e,

$$M_{wS} = (\log_{10} A_{\mathrm{a}} + 4.393)/0.991\,, \tag{2}$$

$$M_{wML} = (\log_{10} A_{\mathrm{a}} + 5.518)/1.137\,, \tag{3}$$

$$M_{wMVL} = (\log_{10} A_{\mathrm{a}} + 6.013)/1.146\,, \tag{4}$$

and the one proposed by Ramírez-Gaytán et al. (2014), specifically developed for subduction events in México

$$M_{wR} = (2/3) * (\log_{10} A_{\mathrm{a}}/(7.78 * 1.0e-9)^{(1/0.550)}) - 6.07\,. \tag{5}$$

In these equations, A_{a} is the area [km^2] of each earthquake generated in the seismic region or domain Ω according to the nomenclature of TREMOL (Monterrubio-Velasco et al., 2019a). Relation in Eq. 2 was obtained from asperities defined by the average displacement criterion (Somerville et al., 1999a). Relations in Eqs. 3 and 4 were found by using the maximum displacement criterion for a large and a very large, asperity, respectively (Mai et al., 2005).

https://doi.org/10.5194/gmd-2020-115
Preprint. Discussion started: 14 July 2020


Geoscientific Model Development Discussions
Open Access
EGU

105 To determine the seismicity curve of a given SA region, TREMOL computes, as a part of the postprocessing, the frequency-magnitude distribution associated with this region. In the case of the SUB3 region, (Zúñiga et al., 2017) discuss the singular behavior followed by the frequency-magnitude distribution, according to the observed data. In the next section, we briefly comment on that.

3 The SUB3 seismic region: Background and essential data

110 As mentioned above, the SUB3 seismic region is a transitional zone between the Cocos and North America plates' convergence. Large events in SUB3 show simple source-time functions and rupture histories. These features were interpreted by Singh and Mortera (1991) as a plate boundary with simple and homogeneous fault surfaces, where slip takes place on single asperities. Zúñiga et al. (2017) proposed a first order seismic regionalization considering geological, seismo-tectonical and seismicity data. In this work, we focus on the SUB3 region, because this region provides an ideal setting for testing the single asperity 115 paradigm with the aid of TREMOL.

3.1 Reference earthquake data

As basic testing data, we use four subduction earthquakes which occurred in this region, from the database published by Rodríguez-Pérez et al. (2018). Hereafter, this database is referred to as "DB-FiniteFault-2018". We use these events because their epicentral coordinates fall into the SUB3 region, their magnitudes are greater than 6.0, and they occurred after 1988 which 120 is a date that indicates the start of the best recording conditions of the network (Zúñiga et al., 2012). The epicentral location and the necessary seismic information of these four mainshocks are shown in Fig. 4 and Table 1, respectively. Moreover, the spatial representation of the effective area associated with these earthquakes is shown in Fig. 4.

It is important to highlight that, according to results in Rodríguez-Pérez and Ottemöller (2013), the size of an earthquake not only depends on the effective area. It also depends on the size of the asperity, among other possible influential variables. For 125 example, in the case of the four earthquakes reported in Table 1 the maximum effective area is equal to 3488.52 km^2 and is associated to an earthquake of magnitude 7.1, according to Table 2. However, the mainshock with the largest magnitude (7.8) is associated to a smaller effective area of 3086.22 km^2.

3.2 The frequency-magnitude distribution in SUB3

To estimate the earthquake frequency in a given region and time span, the linear relation of the frequency-magnitude (F-M) 130 distribution known as Gutenberg-Richter law (GR), is one of the most employed empirical relations in seismology,

$$\log_{10} N(\geq M) = a - bM\,, \tag{6}$$

where N is the cumulative number of earthquakes greater than a specific magnitude M. The parameters a and b depend on regional tectonic characteristics, such as the seismicity level and the stress distribution (Ozturk, 2012; Evernden, 1970).

https://doi.org/10.5194/gmd-2020-115
Preprint. Discussion started: 14 July 2020


Geoscientific Model Development Discussions

Despite the fact that the GR distribution is widely used, other distributions have also been employed to describe F-M observations. For example, paleoseismological data suggest that a specific fault segment may generate characteristic earthquakes, having a very narrow range of magnitudes, as observed in California (Parsons and Geist, 2009; Schwartz and Coppersmith, 1984) or Japan (Parsons et al., 2018).

A characteristic earthquake model implies a non-linear earthquake frequency-magnitude distribution, highly dominated by the occurrence of a preferred size event that induces low *b* values, or plateaus (Schwartz and Coppersmith, 1984). In such cases, a GR relation is not a good representation, and therefore it is not appropriate to describe the earthquake frequency relation for a that particular region (Aki, 1984; Parsons et al., 2018). Alternatively, depending on the regional tectonics, the size distribution of earthquakes could generate a "mixed" magnitude-frequency distribution (Lay et al., 1982; Dahmen et al., 2001), where the frequency-magnitude fits a GR distribution at intermediate magnitudes, but large events (associated with the characteristic earthquake) depart from a linear GR relation (Lomnitz-Adler, 1985; Dalguer et al., 2004). Studies on the frequency-magnitude distributions of earthquakes in the Pacific subduction zone of Mexico are scarce. Singh et al. (1983) reported that the Gutenberg-Richter relation was not appropriate to model the occurrence of large earthquakes in the Mexican subduction zone. They found that the G-R relation in the range $4.5 \leq M_s \leq 6.0$, when extrapolated, grossly underestimated the observed frequency of large earthquakes ($M_s \geq 6.5$) for the Oaxaca and Jalisco regions. Recently, the study performed by Zúñiga et al. (2017) confirmed that the frequency-magnitude distribution in the Mexican subduction zone is not well described by a unique linear GR relation, particularly, at the SUB3 region. These authors described the singular frequency-magnitude relation depicted in Fig. 5, based on data that spans the period 1988-2014. This distribution shows a highly distinctive feature, such as an abrupt change of the frequency-magnitude tendency at the magnitude range $6.4 \leq M_s \leq 7.3$. This feature has been interpreted as the result of seismic events rupturing similar asperities. These repeating earthquakes of similar magnitudes have been identified as “characteristic” events of that system (Singh et al., 1983). During the past 100 years large events were registered in this area, such as in 15 April 1907 (M_s 7.7), 26 March 1908 (M_s 7.6), 17 June 1928 (M_s 7.8), 9 October 1928 (M_s 7.6), 23 December 1937 (M_s 7.5), 28 July 1957 (M_s 7.7), 23 August 1965 (M_s 7.8), 29 October 1978 (M_w 7.8), and 20 March 2012 (M_s 7.5). These earthquakes were strongly felt in cities like Acapulco, Oaxaca, and Mexico, causing some cases significant damages.

4 Methodology

The SUB3 region is approximately delineated by the polygon shown in Fig. 3. To validate our synthetic results, we extract earthquake (magnitude and epicenter) data from the catalog of the Mexican SSN (2019) from 1988. Hereafter we refer to this catalog as "SSN-1988-2018". In order to numerically test the main hypothesis of this work, namely that the seismicity of SUB3 as mainly originated from ruptures at single asperities, we apply the following global framework.

https://doi.org/10.5194/gmd-2020-115
Preprint. Discussion started: 14 July 2020


Geoscientific Model Development Discussions
Open Access
EGU

4.1 Global TREMOL framework: single asperity and aggregated curves

1. Using the database"DB-FiniteFault-2018", we identified all earthquakes with a magnitude greater or equal than 6.5 and occurred within the SUB3 region after 1988. As a result, only four mainshocks satisfy these criteria whose hypocenters are illustrated in Fig. 3. Specifically, we require the data summarized in Table 1. Notice that each of these earthquakes has associated a maximum asperity area, which at the same time, defines a SA region of size $A_{\rm eff}$ each one, depicted in Fig. 4 (as described in subsection 2).

2. We apply TREMOL v0.1.0 to simulate the seismic activity at each SA region. Even though these SA regions are depicted as simple rectangles in Fig. 4, the fault dip and epicentral depth are implicitly considered in TREMOL simulations since the synthetic activity can be seen as a 3-dimensional projection into a bidimensional plane. The dates of the mainshocks and duration of associated seismicity are well separated in time, so that we can consider each SA region as independent for an individual TREMOL simulation.

3. We finally add the four individual synthetic curves to obtain an aggregated seismicity curve for the study area. This area corresponds to 15%-20% of the SUB3 region, approximately.

In the upcoming, we describe further details of this calculation procedure based on TREMOL, and we base our discussion on comparisons of synthetic results with observed seismicity.

4.2 Input parameters and realizations

A TREMOL simulation of each one of the four mainshock earthquakes given in Table 1, requires the values of $L_{\rm eff}$ and $W_{\rm eff}$, also given there, as well as the asperity size $A_{\rm a}$ of each SA region, that is easily determined from $S_{\rm a}$ and $A_{\rm eff}$. A few additional input parameters are specified below. An important consideration relates the uncertainty quantification on the real size of the large and single asperity at each study region. We perform 20 realizations at each SA region by changing the random parameter of the modeled asperity size given by Eq. 1, and then we average these results. The number of 20 realizations was chosen because we estimated by statistical testing that the standard error is invariant for more than 5 realizations, so we consider that 20 is enough to provide a robust statistical outcome. The following are the steps for our numerical test:

1. Defining the input model parameters required by TREMOL. In addition to values given in Table 1, TREMOL also employs as parameters $\pi_{\rm asp} = 0.90$, $\gamma_{\rm asp}$ = 4, and the total number of cells $N_{\rm cell} = 40000$ to define the model domain and characteristics. The number of cells represents a $N_{\rm x} \times N_{\rm y}$ discretization of the fault plane that follows its real aspect ratio given by $\chi = L_{\rm eff}/W_{\rm eff}$ due to the relations,

$$N_{\rm y} = \sqrt{\frac{N_{\rm cell}}{(W_{\rm eff}/L_{\rm eff})}}\,, \quad \text{and} \quad N_{\rm x} = (W_{\rm eff}/L_{\rm eff}) \times N_{\rm y}\,, \tag{7}$$

where $N_{\rm x}$ and $N_{\rm y}$ are the number of cells along the horizontal and vertical direction, respectively.

https://doi.org/10.5194/gmd-2020-115
Preprint. Discussion started: 14 July 2020


Geoscientific Model Development Discussions

2. As statistical support to our resulting curves, we execute TREMOL v0.1 twenty times per each SA region listed in Table 1. At each execution, the asperity size is modified according to the Eq. 1. At the end of each realization, the rupture area of each synthetic event is customarily calculated by TREMOL, and then its equivalent magnitude is computed using Eqs. 2, 3, 4, and 5.

3. For each realization, we also compute the frequency-magnitude distribution of synthetic earthquakes. To do so, we split the magnitude range $M_w \in [2.5, 9]$ into 65 subintervals and count the number of these synthetic events at each magnitude bin. Once the twenty executions for a single SA region have been completed, we also compute the mean and standard deviations of the number of earthquakes at each magnitude bin.

4. Finally, after the four SA simulation sets have been computed, we add their contribution, in the frequency-magnitude range, to the aggregated seismicity curve, considering their mean and standard deviation. This global curve represents the synthetic seismicity of a seismic area about 15%-20% of the whole SUB3 region.

4.3 Observed seismicity distribution

As basis for comparison for TREMOL output, we compiled the distribution of seismicity from a seismic catalogue SSN-1988-2018 of 34716 events that occurred at the SUB3 region from 1988 to 2018 with a minimum magnitude of 1.5 M_w. We extracted from this catalog the events that satisfy the following criteria:

1. The epicentral latitude and longitude coordinates must be within the study regions, according to Fig. 4.

2. They should fall within the reference depth which corresponds to the mainshock hypocenter depth. We included all events in a range of 8 km above and below the mainshock depth to account for the uncertainty on this value, which is a well-known limitation on the hypocentral location. Moreover, in the case of the 25/02/1996 earthquake, we considered all events regardless of their depth, because of the lack of data in the reference catalogue (**SSN-1988-2018**).

3. The occurrence time should fall into the temporal window given by the catalog start date (1/1/1988) and until half a year after the corresponding mainshock date.

The above selection criteria agree with the phenomenology simulated by TREMOL, which aims to model the previous seismic activity up to the mainshock, and in some cases, a few events just after its occurrence since the simulation ends when the area of $S_{\mathrm{a-Asp}}$ is completely activated (ruptured). In this version, TREMOL simulations are limited to bidimensional domains (modeling a dipping fault plane), hence we necessarily have to use a hypocentral depth range for event acceptance. Thus, our consideration to include events ± 8 km from the hypocenter depth is reasonable.

Lastly, it is worth mentioning that, when we construct the aggregated curve of the observed seismicity on the four SA regions of Fig. 4, we take into account each event only once, in the case of the overlapping areas, such as SA regions 1 and 4, or for the case of SA regions 3 and 2.

https://doi.org/10.5194/gmd-2020-115
Preprint. Discussion started: 14 July 2020


Geoscientific Model Development Discussions

5 Results

5.1 Synthetic seismicity distributions

We obtained four synthetic curves computed at each SA region according to the four area-magnitude relations (Eqs. 2, 3, 4, and 5). In Figs. 6, 7, 8 and 9 the blue line represents the real curve obtained from the earthquake catalogue referred in Section 4.3 (SSN-1988-2018), and black curves correspond to synthetic results, where the mean curve of the twenty TREMOL realizations is shown by the solid line, while the dotted lines indicate the standard deviation.

The SA region 1 has approximately an area equal to 3207 km^2 (Table 1), and Fig. 6 shows the observed and TREMOL synthetic seismicity curves. Each subplot in this figure shows a synthetic frequency-magnitude curve obtained for a particular area-magnitude relation (Eqs. 2, 3, 4, and 5). Thus, differences between these four seismicity curves are only attributable to the alternative area-magnitude relations used as a basis in their computation. In this particular region, Eq.5 leads to the frequency-magnitude curve that best matches the observed one. The best fit in this curve is for magnitudes greater than 4.0. The second best approximation corresponds to the case of Eq. 2, whose fit improves for magnitudes greater than 5.5. The third best fit is achieved by Eq. 3 for magnitudes greater than 6, and finally, the worst approximation is given by Eq. 4 with reasonable results only for magnitudes near 7.

A similar analysis can be done for the other SA regions. According to the results for region 2 in Fig. 7, we observe that the best fit is obtained by the application of Eq. 5 (lower right subplot). In this case, the synthetic seismicity curve closely approaches the observed data for magnitudes greater than 4.0. Results for region 3 depicted in Fig. 8, indicate that the best synthetic fit is achieved by the curve computed from Eq. 2, particularly, for magnitudes greater than 4.5. We can also observe that the poorest fit is obtained by using Eq. 5, which underestimates the real seismicity. Finally, TREMOL′s results for region 4 in Fig. 9 reveal the excellent fit attained by the application of Eq. 5. This latter result is the best fit overall, but we highlight the fact that this region includes the largest number of observed events.

5.2 Synthetic aggregated curves

Aiming at approximating the seismicity of nearly 15%-20% of the SUB3 region, as mentioned in Section 4, we added the four synthetic SA curves previously computed into an aggregated single curve. We consider this part of the analysis a useful validation of our methodology based on TREMOL, providing important insight into the hypothesis of single asperity ruptures and its relation with real cases. Fig. 10 shows the aggregated seismicity curves, each one based on results corresponding to a particular magnitude-area relationship (Eqs. 2 - 5). In this figure, we observe that the synthetic curve based on Eq. 5, more closely matches the real seismicity curve for magnitudes larger than 4, while the other scaling relations only approach the observed seismicity curves for M >6.

https://doi.org/10.5194/gmd-2020-115
Preprint. Discussion started: 14 July 2020

Geoscientific Model Development Discussions

6 Effects of the aspect ratio χ on the frequency-magnitude distributions.

In what follows we discuss the sensitivity of the model to the aspect ratio $\chi = L_{\rm eff}/W_{\rm eff}$ as reflected in the shape of the F-M distributions.

Previous observational and numerical studies have implied a direct relation of the fault aspect ratio over the frequency-magnitude distribution (Weng and Yang, 2017; Yoder et al., 2012; Stock and Smith, 2000; Main, 2000, 1995; Main and Burton, 1989; Console et al., 2015; Tejedor et al., 2009; Heimpel, 2003). These works motivated us to conduct a study of the effect of the aspect ratio on the main characteristics of the F-M distributions generated by our model. With this in mind, we carried out a comparison between our results and those found by using different approaches. First, we define two equations that assign the number of cells according to the width $N_{\rm y}$ and length $N_{\rm x}$ of the domain.

$$N_{\rm x} = (W_{\rm eff}/L_{\rm eff}) \times R_{\rm a} \times L^*\,, \quad \text{and} \quad N_{\rm y} = N_{\rm cell}/N_{\rm x}\,, \tag{8}$$

We define the aspect factor $R_{\rm a}$ as a value that extends the $N_{\rm x}$ side of the rectangle, assigning the number of cells in the width and length sizes of the domain, $L^* = \sqrt{N_{\rm cell}}$. As $R_{\rm a}$ increases the aspect ratio χ transforms the domain area into a thinner rectangle. Eq. 8 allows us to compare different aspect ratio values preserving the number of cells $N_{\rm cell}$.

To perform this study, we chose as reference the fourth SA region because its width-length ratio is close to 1 (1.03), *i.e.,* making it a squared source ($L_{\rm eff}/W_{\rm eff} = 1$). In the experiment, we modified the ratio $R_{\rm a}$ (as is observed in Fig. 11) in the algorithm, keeping constant the number of cells in the computational domain, $N_{\rm cell} = 10000$, as well as the other input parameters. In this work, we consider values of $R_{\rm a} \geq 1$. The values of χ for the four seismic regions are shown in Table 2). It is worth mentioning that the aspect factor $R_{\rm a}$ modifies the effective area and the asperity region in the same proportion.

In Fig. 11 we exemplify two different $R_{\rm a}$ and their respective χ values, being (a) $R_{\rm a} = 1$ and $\chi = 1.0$, (b) $R_{\rm a} = 2$ and $\chi = 3.8$, considering the same number of cells ($N_{\rm cell} = 10000$). The color bar indicates the strength value γ, with one corresponding to the minimum value assigned to the background area. The simulated asperity has a heterogeneous strength $\gamma_{\rm asp}$, which is also larger than the background.

6.1 Results of the Aspect Ratio influence

The aim of this part of the analysis was to explore the effect of the fault aspect ratio $R_{\rm a}$ on the synthetic (frequency-magnitude) seismicity generated by TREMOL. In Fig. 12 we plot magnitude-frequency histograms for six different aspect ratios: Fig. 12 (a) $R_{\rm a} = 1$, Fig. 12 (b) $R_{\rm a} = 1.4$, Fig. 12 (c) $R_{\rm a} = 1.7$, Fig. 12 (d) $R_{\rm a} = 2.0$, Fig. 12 (e)$R_{\rm a} = 2.1$, and Fig. 12 (f) $R_{\rm a} = 2.4$. Fig. 12 illustrates the strong dependency of the frequency-magnitude distribution on the χ value. In our model, this distribution reaches a critical point for values of $R_{\rm a} > 2.0$ ($\chi > 3.8$), at whose value TREMOL generates only a few events of large magnitude. The behavior of the synthetic seismicity displayed in Fig. 12 is very interesting and shows a possible relation of the area size in the transition between a GR distribution-type behavior and a "characteristic" type. In our results, we pointed out that the maximum magnitude in the six cases is well constrained. In that sense, we could conclude that the maximum magnitude is related to the

https://doi.org/10.5194/gmd-2020-115
Preprint. Discussion started: 14 July 2020


Geoscientific Model Development Discussions

total rupture area and not to its aspect ratio or shape. However, as seen in the figure, the decrease and/or lack of lower magnitude events strongly depends on the aspect ratio. The aspect ratio has been found to play a crucial role in empirical and numerical studies. For example, Tejedor et al. (2009) argues that the aspect ratio is important in real faults because it is appears to have direct relation with the overall size of the fault plane, i.e. small faults being roughly square with and aspect ratio, $\chi \approx 1$, whilst big faults being elongated with aspect ratio, $\chi > 1$, due to the depth limit that the brittle-ductile transition imposes on the Earth crust (around 15 km for vertical strike-slip faults, and twice that for subduction-type faults). Considering this depth limit and the range of surface fault trace lengths (from few kilometers for small earthquakes to hundredths of km for great earthquakes), a reasonable range of aspect ratios for real faults is $1 < \chi < 5$. Main (2000), considers that even the largest earthquakes have a fairly constant aspect ratio of around 2, the scatter ranges between 1 and 4. Stock and Smith (2000) show that the aspect ratio of dip-slip earthquakes is similar for all earthquake sizes. Hence, the limitation in rupture width seems to control the maximum possible rupture length for these events. They also found, after analyzing the case of five earthquakes, that only one normal event (31/6/1970, Columbia, M_w = 7.7) and four reverse events (09/03/1957, Aleutians, M_w= 8.25; 22/05/1960, Chile, M_w= 8.5; 04/02/1965, Rat Island, M_w= 8.25; 29/09/1973, Vladivostok,M_w= 7.75) had a rupture length to width ratio larger than 4. Heimpel (2003) conducted a study via numerical simulations about the change in frequency-magnitude because of the aspect ratio. They found a similar behavior where for large χ quasi-periodically rupture the entire fault and smaller events do not occur. They pointed out that it happens because, in its models, the characteristic length of large events have an aspect ratio approaching that of the entire fault. In the case of strike-slip fault type Heimpel (2003) found larger values of χ. The seismogenic widths of strike-slip faults are usually less than 20-30 km according to the finite fault rupture models of earthquakes (Weng and Yang, 2017). In our results, the four mainshocks analyzed in this work (Table 1) have χ values between 1 and 2, and therefore, their magnitude-frequency histograms are similar to Fig. 12 (a) and (b). Those values agree with the results found in the referred previous works.

7 Discussion

The simulated seismicity distributions obtained through TREMOL show a high similarity to real seismicity curves associated with the four SUB3 reference mainshocks, for magnitude values of $M_w \geq 4$, if a proper scaling magnitude-area relation is adopted (see Figs. 6, 7, 8, 9, and Fig. 10). In three of these reference cases, the best relationship is the one proposed by Ramírez-Gaytán et al. (2014), which leads to an excellent fit in the referred magnitude range (see Figs. 6, 7, and 9). Alternatively, there is one case where a better fitting is achieved by using the relation proposed by Somerville et al. (1999b) (see Fig. 8). Finally, the synthetic aggregated curves in Fig. 10 show that the scaling of Ramírez-Gaytán et al. (2014) in Eq. 5 allows a better global fit when considering the four SA regions in SUB3. This relation was developed using $M_w \in$ [6.9-8.1] earthquakes in the Mexican subduction zone, hence it seems reasonable that this relation works well for the main events studied in this paper.

It is worth pointing out the cases including events of magnitude lower than $M_w = 4$, where synthetic curves usually overestimate the real seismicity curves (Figs. 6, 7, 8, 9, and 12). This may occur because the number of events in the seismic catalog is not enough to compare with the synthetic ones due to the limitations of the network. In support of this assumption, we

https://doi.org/10.5194/gmd-2020-115
Preprint. Discussion started: 14 July 2020

Geoscientific Model Development Discussions
Open Access
EGU

emphasize the results for the 2012 mainshock that has the largest number of associated events, since it was for this case that TREMOL was able to more closely match the observed distribution even for small magnitudes of $M_w \geq 3$.

In summary, we can conclude that the synthetic seismicity distributions agree well with the observations related to the four earthquakes of magnitude $M_w > 4$ used as study cases. The good agreement achieved by the synthetic frequency-magnitude curves, support the assumption in Zúñiga et al. (2017) that attribute this type of distribution to ruptures of single asperities and provide further support to the hypothesis that regions where ruptures are simple, yield relations that depart from the linearity of the common G-R law, indicating a process of characteristic events. Moreover, as a way to provide an additional counterexample of the capabilities of TREMOL in the case of absence of a hard asperity area, we modeled the expected seismicity on the SA region 4 under uniform π and γ values. We allow for these conditions by taking $\pi_{\text{asp}} = \pi_{\text{bkg}} = 0.67$, and $\gamma_{\text{asp}} = \gamma_{\text{bkg}} = 1$. Fig. 1 compares this new synthetic frequency-magnitude curve, in the absence of a hard asperity, with the previous TREMOL result that accounts for a single asperity (and shown in Fig. 9), and the real seismicity. Fig. 1 proves that the asperity condition in TREMOL is indeed a mandatory requirement to reproduce the seismicity features observed in the SUB3 region.

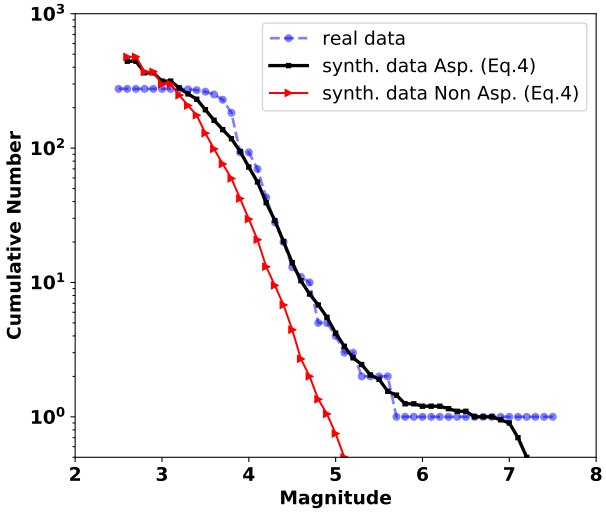

Figure 1. The real and TREMOL frequency-magnitude curves for the SA region 4. The solid black line represents the mean synthetic seismicity curve of 20 realizations considering one single asperity in the domain. The red line corresponds to the mean synthetic seismicity curve of 20 realizations without any single asperity in the domain.

Lastly, TREMOL results in Fig. 12 reveal their sensitivity to the fault aspect ratio χ. As χ increases, *i.e.,* the effective area is modeled as a long-rectangle, the synthetic frequency-magnitude distribution changes until the critical $\chi \approx 4$ value is reached, above which only large magnitude events are triggered. These results indicate that the shape of the modeled asperity controls the frequency-magnitude distribution of the synthetic data. In general, square fault areas allow the generation of a large variety of magnitude events. On the other hand, as the asperity area becomes a long rectangle, TREMOL generates only a few large

https://doi.org/10.5194/gmd-2020-115
Preprint. Discussion started: 14 July 2020


Geoscientific Model Development Discussions

events. Thus, in our model, we can control the transition of the magnitude distribution through the χ parameter. Moreover, our numerical results agree with observational studies that find a similar $\chi \approx 2$ for dip-slip faulting style.

8 Conclusions

The frequency-magnitude distribution has a significant impact on the seismic hazard assessment. Asperities seem to have a direct relation with the occurrence of preferred size events. In this work, we set to demonstrate the capability of the model employed in TREMOL v0.1.0 to generate seismicity distributions similar to those observed in region SUB3 of the subduction regime of Mexico for magnitudes $M_w > 4$. Our simulation results support the hypothesis presented by Singh and Mortera (1991) and Zúñiga et al. (2017) that ascribe mainshocks occurring in region SUB3 as mainly generated from rupture of single asperities (Fig. 1). Nevertheless, we also find an impact on the synthetic curves that depends on the area-magnitude scale relation. We find that in four cases out of five, the relation that better fits the synthetic in relation to the real curve is that proposed by Ramírez-Gaytán et al. (2014). It is worth to note that this relationship was developed for earthquakes from the Mexican subduction zone, hence it is expected to work well to describe the magnitude-area relation of the events simulated in this paper.

TREMOL makes it possible to analyze regions where seismic data is too limited. In this sense, it is worth to note that we use as input data the information of four large earthquakes, but the number of events generated approaches 1000. Furthermore, we find that our model agrees with the results obtained in other studies that emphasize the importance of the fault aspect ratio χ on the frequency-magnitude distribution. Nevertheless, results for the four analyzed sub-seismic regions indicate that the behavior of the synthetic histograms matches well the observed ones in the range $1 \leq \chi < 4$.

Results further encourage us to continue exploring the capabilities of our model, for future applications of TREMOL v0.1.0 for the modeling of seismicity distributions at other subduction zones, such as Chile or Japan. In addition, we continue working on more general rupture models by including tridimensional fault systems, as well as a reloading process that allows the generation of the seismic cycle.

Code availability. The TREMOL code is freely available at GitHub repository (https://github.com/monterrubio-velasco), or by requesting the author (marisol.monterrubio@bsc.es). In all cases, the code is supplied in a manner to ease the immediate execution under Linux platforms. Preprocessing, run control and postprocessing scripts covering every data processing action for all the results reported in this work is provided https://github.com/monterrubio-velasco/TREMOL_singlets/tree/TREMOL_singlets_SUB3study. User's manual documentation are provided in the archive as well.

Data availability. Data sets are available through Monterrubio-Velasco et al. (2019a), Rodríguez-Pérez et al. (2018), and SSN (2019).

https://doi.org/10.5194/gmd-2020-115
Preprint. Discussion started: 14 July 2020

Author contributions. MMV developed TREMOL v0.1.0 code and the methodology used in this paper. MMV, RZ, AAM, OR, QRP and JP provided guidance and theoretical advice during the study. All the authors contributed to the analysis and interpretation of the results. All the authors contributed to the writing and editing of the paper.

Competing interests. The authors declare that they have no conflict of interest.

Acknowledgements. The research leading to these results has received funding from the European Union's Horizon 2020 research and innovation programme under the grant agreement Nº 823844, ChEESE CoE Project (last access: 19 April 2020). M. Monterrubio-Velasco, O. Rojas and J. de la Puente thanks to ChEESE CoE Project. Quetzalcoatl Rodríguez-Pérez was supported by the Mexican National Council for Science and Technology (CONACYT) (Cátedras program- project 1126).

https://doi.org/10.5194/gmd-2020-115
Preprint. Discussion started: 14 July 2020

References

Aki, K.: Asperities, barriers, characteristic earthquakes and strong motion prediction, Journal of Geophysical Research: Solid Earth, 89, 5867–5872, 1984.

Blaser, L., Krüger, F., Ohrnberger, M., and Scherbaum, F.: Scaling relations of earthquake source parameter estimates with special focus on subduction environment, Bulletin of the Seismological Society of America, 100, 2914–2926, 2010.

Console, R., Carluccio, R., Papadimitriou, E., and Karakostas, V.: Synthetic earthquake catalogs simulating seismic activity in the Corinth Gulf, Greece, fault system, Journal of Geophysical Research: Solid Earth, 120, 326–343, 2015.

Cornell, C. A.: Engineering seismic risk analysis, Bulletin of the seismological society of America, 58, 1583–1606, 1968.

Dahmen, K., Fisher, D., Ben-Zion, Y., Ertas, D., and Ramanathan, S.: Gutenberg-Richter and characteristic earthquake behavior in Simple Models of Heterogeneous Faults, in: AGU Spring Meeting Abstracts, 2001.

Dalguer, L. A., Miyake, H., and Irikura, K.: Characterization of dynamic asperity source models for simulating strong ground motion, in: Proceedings of the 13th World Conference on Earthquake Engineering, 3286, Citeseer, 2004.

Evernden, J.: Study of regional seismicity and associated problems, Bulletin of the Seismological Society of America, 60, 393–446, 1970.

Hansen, A., Hemmer, P. C., and Pradhan, S.: The fiber bundle model: modeling failure in materials, John Wiley & Sons, 2015.

Heimpel, M.: Characteristic scales of earthquake rupture from numerical models, 2003.

Lay, T., Kanamori, H., and Ruff, L.: The asperity model and the nature of large subduction zone earthquakes, na, 1982.

Lei, X.: How do asperities fracture? An experimental study of unbroken asperities, Earth and Planetary Science Letters, 213, 347–359, 2003.

Lomnitz-Adler, J.: Asperity models and characteristic earthquakes, Geophysical Journal International, 83, 435–450, 1985.

Mai, P. M. and Beroza, G. C.: Source scaling properties from finite-fault-rupture models, Bulletin of the Seismological Society of America, 90, 604–615, 2000.

Mai, P. M., Spudich, P., and Boatwright, J.: Hypocenter locations in finite-source rupture models, Bulletin of the Seismological Society of America, 95, 965–980, 2005.

Main, I.: Apparent breaks in scaling in the earthquake cumulative frequency-magnitude distribution: fact or artifact?, Bulletin of the Seismological Society of America, 90, 86–97, 2000.

Main, I. G.: Earthquakes as critical phenomena: implications for probabilistic seismic hazard analysis, Bulletin of the Seismological Society of America, 85, 1299–1308, 1995.

Main, I. G. and Burton, P. W.: Seismotectonics and the earthquake frequency-magnitude distribution in the Aegean area, Geophysical Journal International, 98, 575–586, 1989.

Monterrubio-Velasco, Rodríguez-Pérez, Q., Zúñiga, F. R., Scholz, D., Aguilar-Meléndez, A., and de la Puente, J.: A stochastic rupture earthquake code based on the fiber bundle model (TREMOL v0.1): application to Mexican subduction earthquakes, Geoscientific Model Development, 2019a.

Monterrubio-Velasco, Zúñiga, F. R., Carrasco-Jiménez, J. C., Márquez-Ramírez, V., and de la Puente, J.: Modeling active fault systems and seismic events by using a fiber bundle model–example case: the Northridge aftershock sequence, Solid Earth, 10, 1519–1540, 2019b.

Murotani, S., Miyake, H., and Koketsu, K.: Scaling of characterized slip models for plate-boundary earthquakes, Earth, planets and space, 60, 987–991, 2008.

Ozturk, S.: Statistical correlation between b-value and fractal dimension regarding Turkish epicentre distribution, Earth Sciences Research Journal, 16, 2012.

https://doi.org/10.5194/gmd-2020-115
Preprint. Discussion started: 14 July 2020

Parsons, T. and Geist, E. L.: Is there a basis for preferring characteristic earthquakes over a Gutenberg–Richter distribution in probabilistic earthquake forecasting?, Bulletin of the Seismological Society of America, 99, 2012–2019, 2009.

Parsons, T., Geist, E. L., Console, R., and Carluccio, R.: Characteristic earthquake magnitude frequency distributions on faults calculated from consensus data in California, Journal of Geophysical Research: Solid Earth, 123, 10–761, 2018.

Pradhan, S., Hansen, A., and Chakrabarti, B. K.: Failure processes in elastic fiber bundles, Reviews of modern physics, 82, 499, 2010.

Ramírez-Gaytán, A., Aguirre, J., Jaimes, M. A., and Huérfano, V.: Scaling relationships of source parameters of M w 6.9–8.1 earthquakes in the Cocos–Rivera–North American subduction zone, Bulletin of the Seismological Society of America, 104, 840–854, 2014.

Rodríguez-Pérez, Q. and Ottemöller, L.: Finite-fault scaling relations in México, Geophysical Journal International, 193, 1570–1588, 2013.

Rodríguez-Pérez, Q. and Zúñiga, F.: Seismicity characterization of the Maravatío-Acambay and Actopan regions, central Mexico, Journal of South American Earth Sciences, 76, 264–275, 2017.

Rodríguez-Pérez, Q., Márquez-Ramírez, V., Zúñiga, F., Plata-Martínez, R., and Pérez-Campos, X.: The Mexican Earthquake Source Parameter Database: A New Resource for Earthquake Physics and Seismic Hazard Analyses in México, srl, 89, 1846–1862, 2018.

Ruff, L. J.: Asperity distributions and large earthquake occurrence in subduction zones, Tectonophysics, 211, 61–83, 1992.

Schwartz, D. P. and Coppersmith, K. J.: Fault behavior and characteristic earthquakes: Examples from the Wasatch and San Andreas fault zones, Journal of Geophysical Research: Solid Earth, 89, 5681–5698, 1984.

Singh, S. and Mortera, F.: Source time functions of large Mexican subduction earthquakes, morphology of the Benioff zone, age of the plate, and their tectonic implications, Journal of Geophysical Research: Solid Earth, 96, 21 487–21 502, 1991.

Singh, S., Rodriguez, M., and Esteva, L.: Statistics of small earthquakes and frequency of occurrence of large earthquakes along the Mexican subduction zone, Bulletin of the Seismological society of America, 73, 1779–1796, 1983.

Somerville, P., Irikura, K., Graves, R., Sawada, S., Wald, D., Abrahamson, N., Iwasaki, Y., Kagawa, T., Smith, N., and Kowada, A.: Characterizing crustal earthquake slip models for the prediction of strong ground motion, Seismological Research Letters, 70, 59–80, 1999a.

Somerville, P., Irikura, K., Graves, R., Sawada, S., Wald, D., Abrahamson, N., Iwasaki, Y., Kagawa, T., Smith, N., and Kowada, A.: Characterizing crustal earthquake slip models for the prediction of strong ground motion, Seismological Research Letters, 70, 59–80, 1999b.

SSN: Mexican Seismological Service, http://www2.ssn.unam.mx:8080/sismos-fuertes/, 2019.

Stock, C. and Smith, E. G.: Evidence for different scaling of earthquake source parameters for large earthquakes depending on faulting mechanism, Geophysical Journal International, 143, 157–162, 2000.

Strasser, F. O., Arango, M., and Bommer, J. J.: Scaling of the source dimensions of interface and intraslab subduction-zone earthquakes with moment magnitude, Seismological Research Letters, 81, 941–950, 2010.

Tejedor, A., Gómez, J. B., and Pacheco, A. F.: Earthquake size-frequency statistics in a forest-fire model of individual faults, Physical Review E, 79, 046 102, 2009.

Weng, H. and Yang, H.: Seismogenic width controls aspect ratios of earthquake ruptures, Geophysical Research Letters, 44, 2725–2732, 2017.

Yamanaka, Y. and Kikuchi, M.: Asperity map along the subduction zone in northeastern Japan inferred from regional seismic data, Journal of Geophysical Research: Solid Earth, 109, 2004.

Yazdi, P., Gaspar-Escribano, J. M., Santoyo, M. A., and Staller, A.: Analysis of the 2014 Mw 7.3 Papanoa (Mexico) Earthquake: Implications for Seismic Hazard Assessment, Seismological Research Letters, https://doi.org/10.1785/0220190032, https://doi.org/10.1785/0220190032, 2019.

https://doi.org/10.5194/gmd-2020-115
Preprint. Discussion started: 14 July 2020

Yoder, M. R., Holliday, J. R., Turcotte, D. L., and Rundle, J. B.: A geometric frequency–magnitude scaling transition: Measuring b= 1.5 for large earthquakes, Tectonophysics, 532, 167–174, 2012.

Zúñiga, F. R., Reyes, M. A., and Valdés, C.: A general overview of the catalog of recent seismicity compiled by the Mexican Seismological Survey, Geofísica Internacional, 39, 2012.

Zúñiga, F. R., Suárez, G., Figueroa-Soto, Á., and Mendoza, A.: A first-order seismotectonic regionalization of México for seismic hazard and risk estimation, Journal of Seismology, 21, 1295–1322, 2017.

https://doi.org/10.5194/gmd-2020-115
Preprint. Discussion started: 14 July 2020

Geoscientific Model Development
Discussions
Open Access
EGU

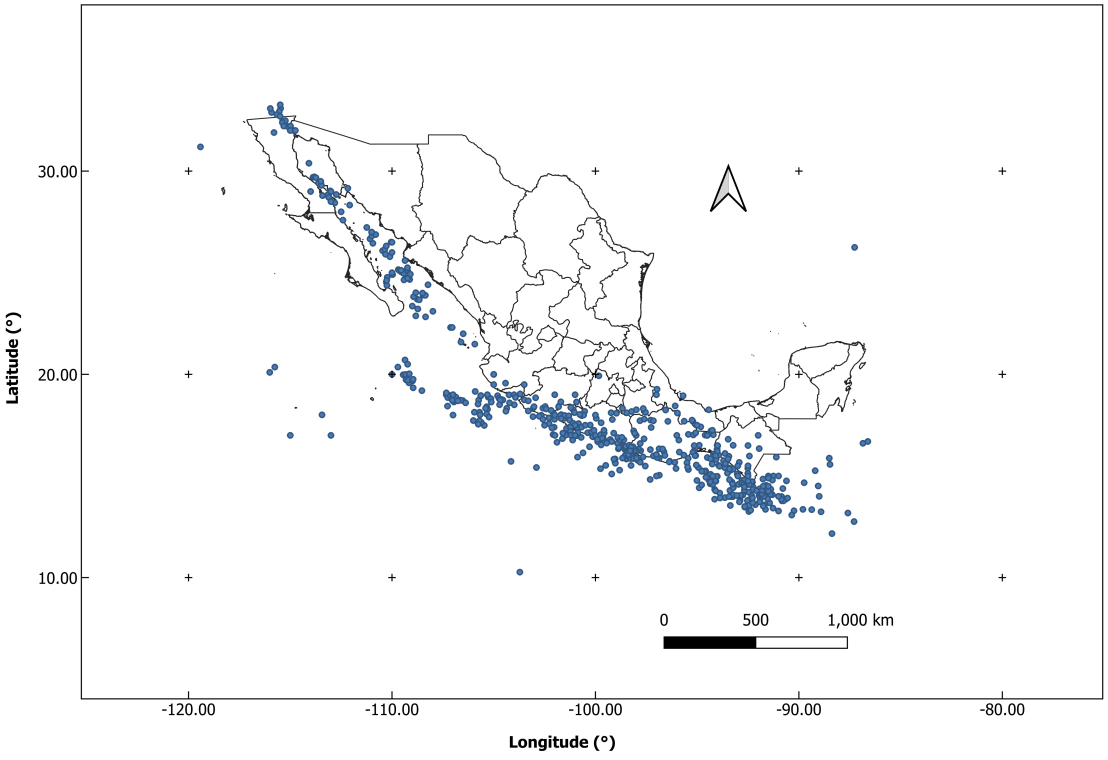

Figure 2. Map of earthquake epicenters in Mexico. From 1900 to 1973, events have magnitudes greater or equal to 6.5, and from 1974 to June 30, 2019, events have magnitudes greater or equal to 5.5 (SSN, 2019)

https://doi.org/10.5194/gmd-2020-115
Preprint. Discussion started: 14 July 2020

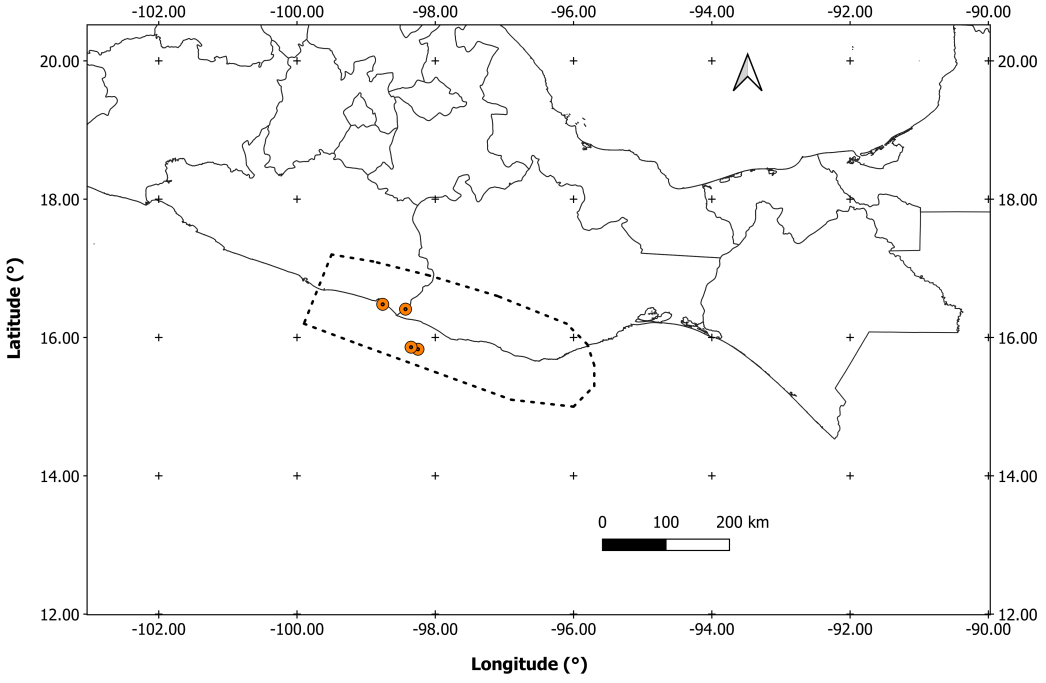

Figure 3. Map of epicenters (orange circles) of the four earthquakes described in Table 1. The SUB3 region is the polygon enclosed by the dotted line.

https://doi.org/10.5194/gmd-2020-115
Preprint. Discussion started: 14 July 2020

Geoscientific Model Development Discussions
Open Access
EGU

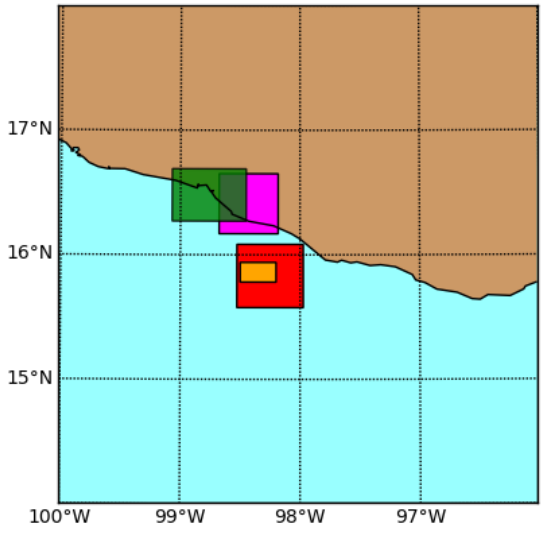

Figure 4. Effective area of the four earthquakes of Table 1.

https://doi.org/10.5194/gmd-2020-115
Preprint. Discussion started: 14 July 2020

Geoscientific Model Development Discussions
Open Access
EGU

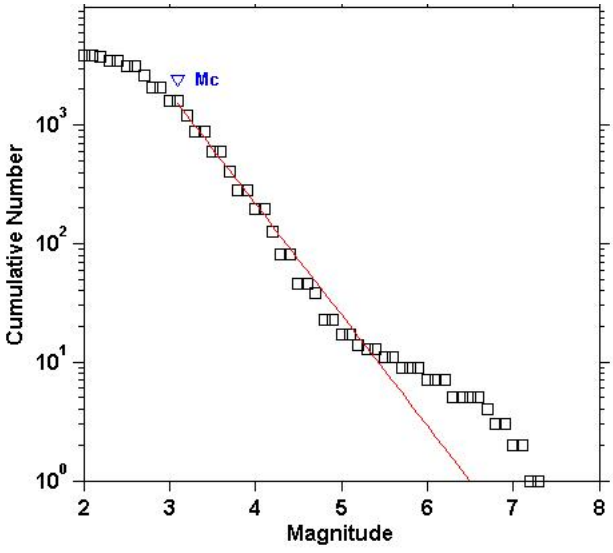

Figure 5. Frequency-magnitude distribution of events occurred in the *SUB3* seismic region (Zúñiga et al., 2017)

https://doi.org/10.5194/gmd-2020-115
Preprint. Discussion started: 14 July 2020

Geoscientific Model Development
Discussions
Open Access
EGU

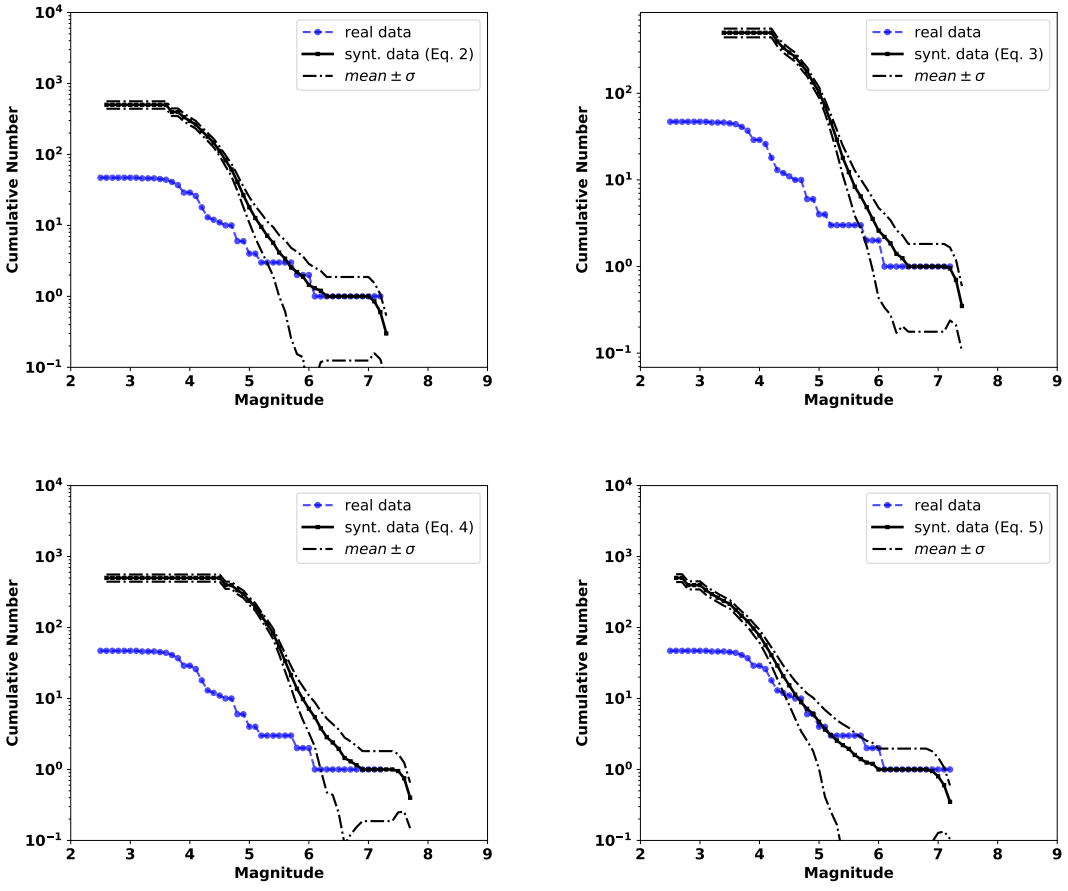

Figure 6. Observed and TREMOL synthetic frequency-magnitude curves for SA region 1 (Table 1). The solid black line indicates the mean after 20 realizations and the broken lines the standard deviation. The blue line is the observed seismicity distribution for events from 1988 to half year before the mainshock date (14/09/1995), including events occurred at the depth range mentioned in the text. Each mean curve is obtained by the application of one of the four magnitude-area relations used in this work: (a) Eq. 2 (upper left subplot), (b) Eq. 3 (upper right subplot), (c) Eq. 4 (lower left subplot), and (d) Eq. 5 (lower right subplot)

https://doi.org/10.5194/gmd-2020-115
Preprint. Discussion started: 14 July 2020

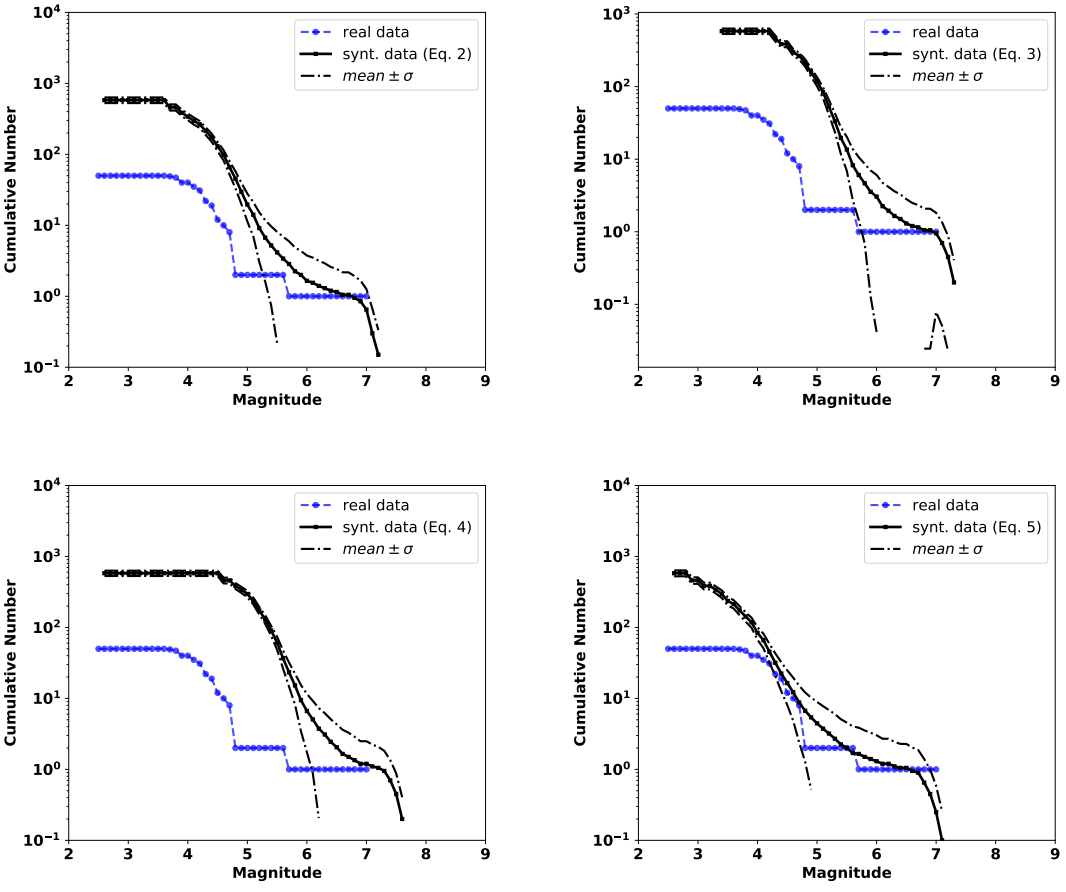

Figure 7. Observed and TREMOL synthetic frequency-magnitude curves for SA region 2 (Table 1). The solid black line indicates the mean after 20 realizations and the broken lines the standard deviation. The blue line is the seismicity curve for events from 1988 to half year before the mainshock date (25/02/1996), including earthquakes occurred at the depth range mentioned in the text. Other features as in Fig. 5.

https://doi.org/10.5194/gmd-2020-115
Preprint. Discussion started: 14 July 2020

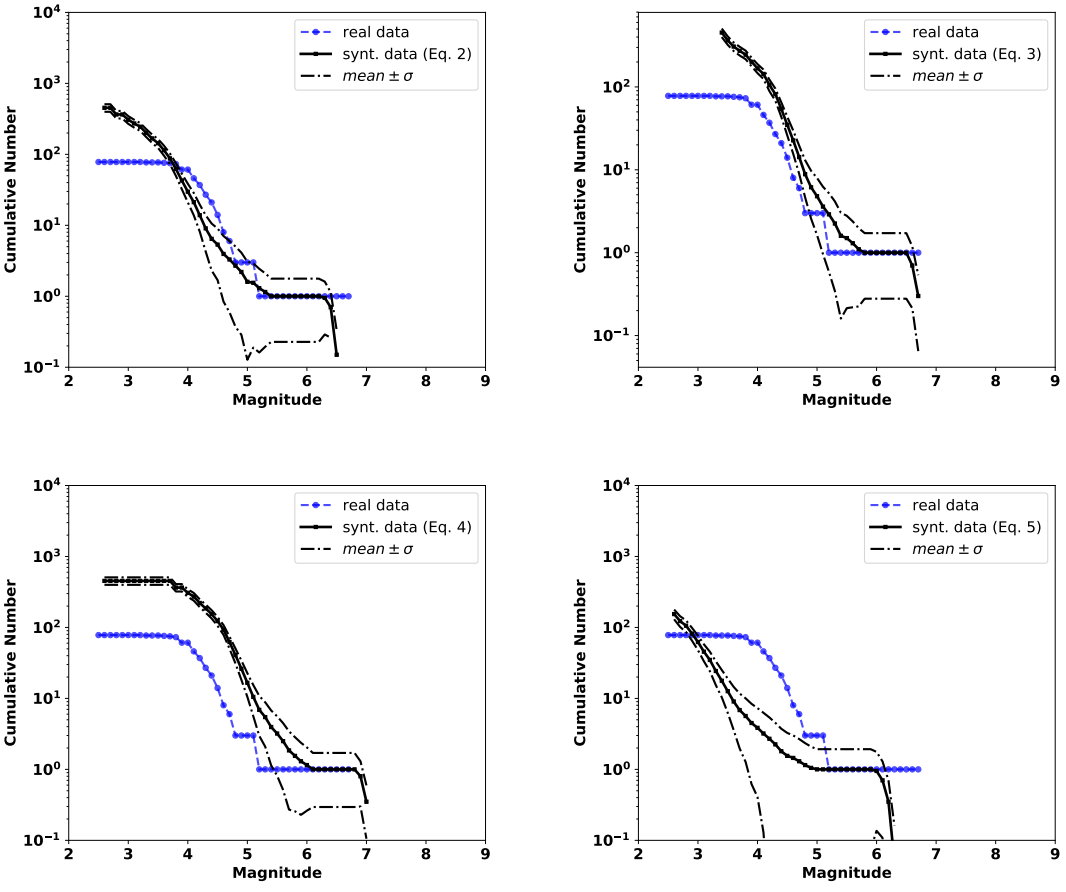

Figure 8. Observed and TREMOL synthetic frequency-magnitude curves for SA region 3 (Table 1). The solid black line indicates the mean after 20 realizations and the broken lines the standard deviation. The blue line is the seismicity curve for events from 1988 to half year before the mainshock date (19/07/1997) including earthquakes occurred at the depth range mentioned in the text. Other features as in Fig. 5.

https://doi.org/10.5194/gmd-2020-115
Preprint. Discussion started: 14 July 2020

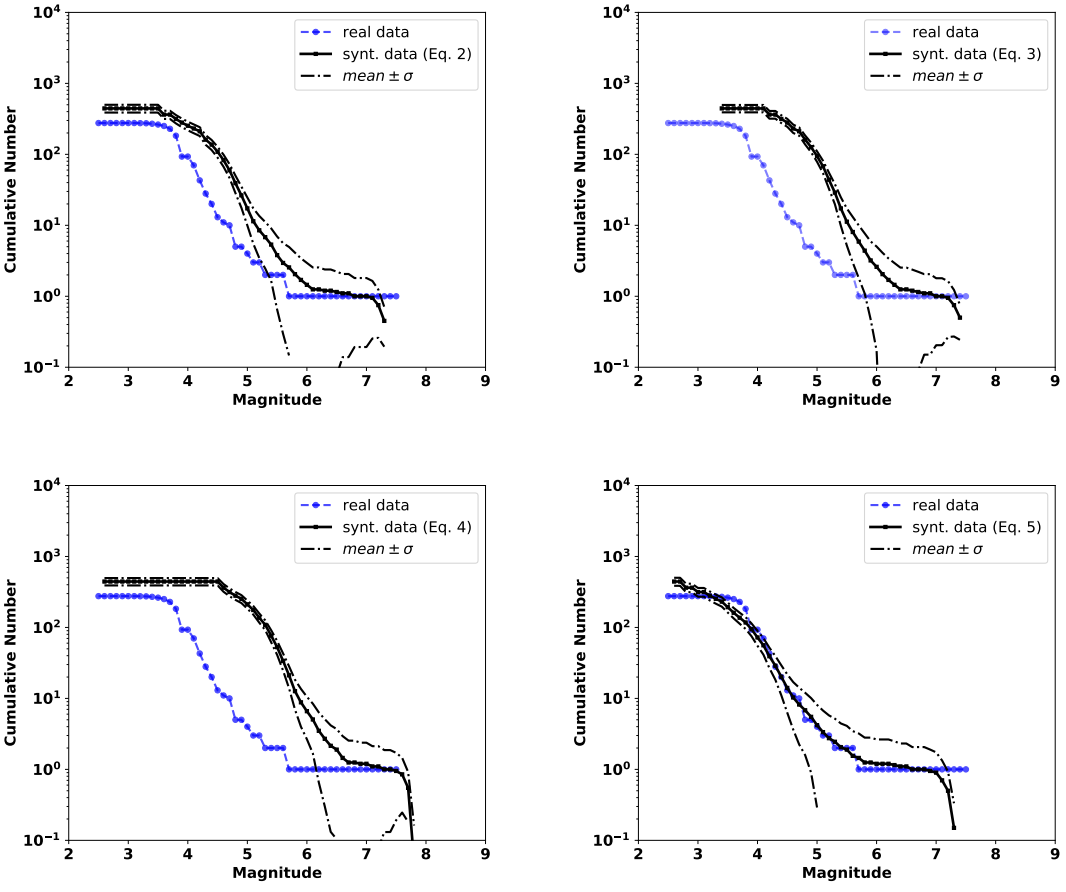

Figure 9. Observed and TREMOL synthetic frequency-magnitude curves for SA region 4 (Table 1). The solid black line indicates the mean after 20 realizations and the broken lines the standard deviation. The blue line is the seismicity curve for events from 1988 to half year before the mainshock date (20/03/2012) including earthquakes occurred at the depth range mentioned in the text. Other features as in Fig. 5.

https://doi.org/10.5194/gmd-2020-115
Preprint. Discussion started: 14 July 2020

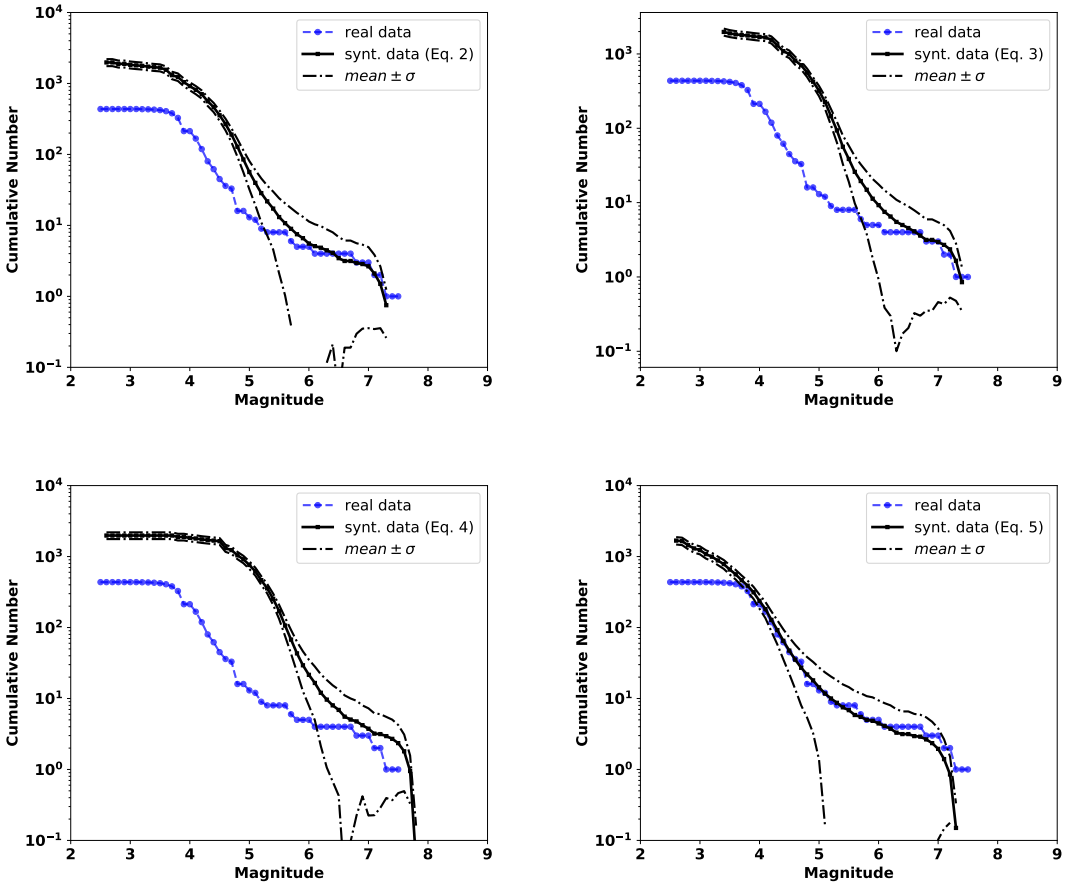

Figure 10. Observed and TREMO synthetic frequency-magnitude curves for the aggregated frequency-magnitude curves computed with the contribution of the four mainshock ruptures. The solid black line is the mean of the synthetic results considering 80 realizations and the broken lines the standard deviation. The blue line is the seismicity curve for events of Figs. 6, 7, 8, and 9. Each mean curve is obtained from one of the four magnitude-area relationships used in this study: (a) Eq. 2 (upper left subplot), (b) Eq. 3 (upper right subplot), (c) Eq. 4 (lower left subplot), and (d) Eq. 5 (lower right subplot)

https://doi.org/10.5194/gmd-2020-115
Preprint. Discussion started: 14 July 2020

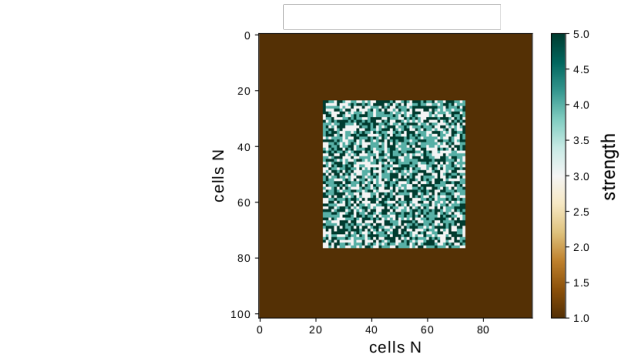

(a)

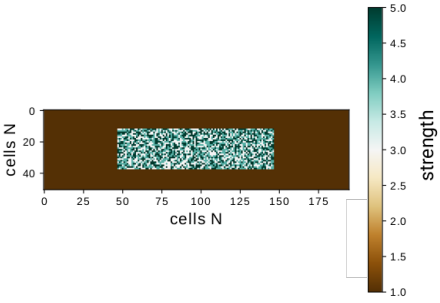

(b)

Figure 11. Example of two sub-seismic regions with different aspect ratio, $\chi = L_{\text{eff}}/W_{\text{eff}}$. The number of cells remains constant in both cases $N_{\text{cell}} = 10000$. (a)$R_{\text{a}} = 1$ and $\chi = 1.0$, (b) $R_{\text{a}} = 2$ and $\chi = 3.8$

https://doi.org/10.5194/gmd-2020-115
Preprint. Discussion started: 14 July 2020

Geoscientific Model Development Discussions

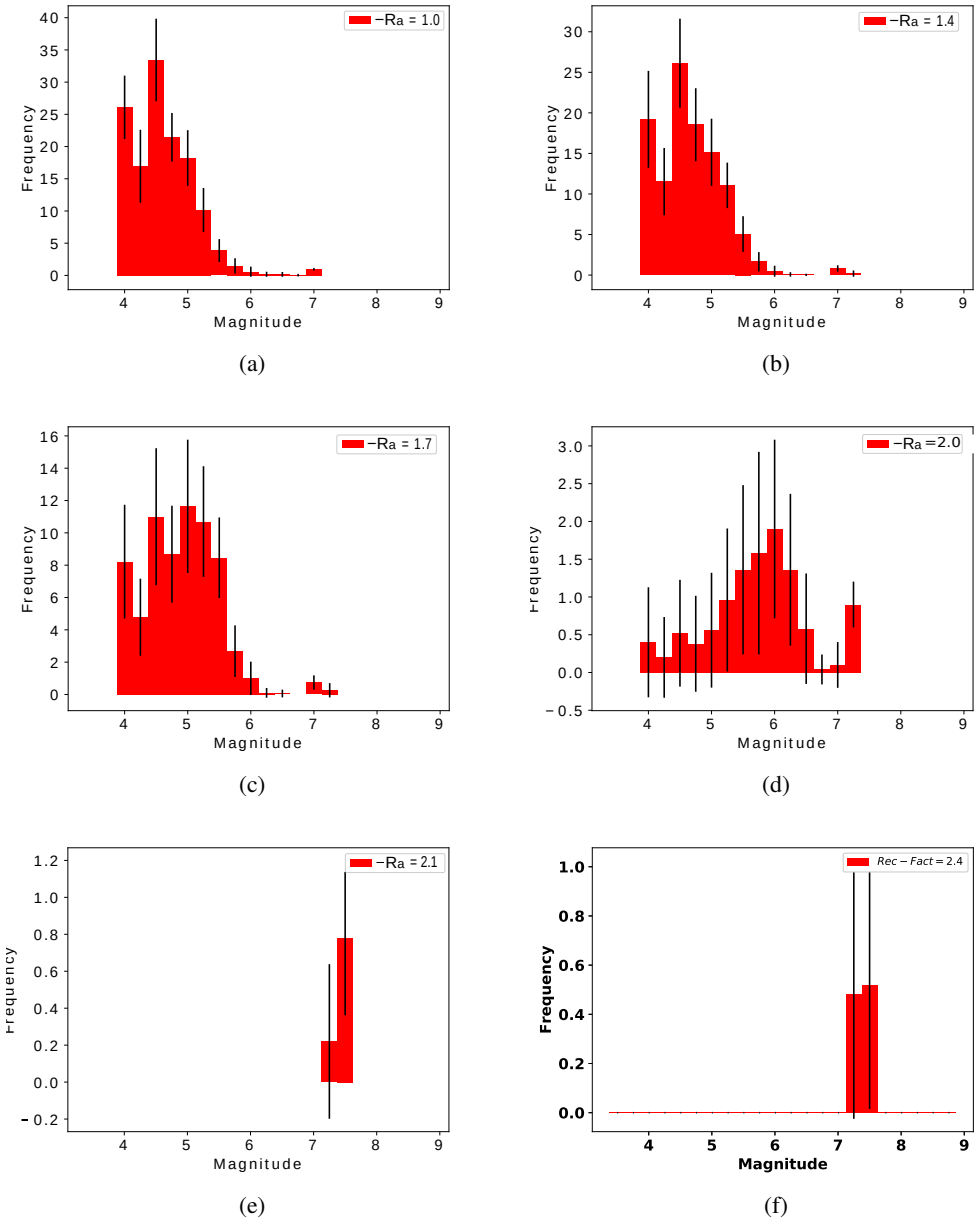

Figure 12. Frequency-magnitude histograms as function of the ratio size R_a and the effective area A_{eff} (Table 1). The bars shows the mean histogram, and the error bars depicts the standard deviation of the twenty realizations.

https://doi.org/10.5194/gmd-2020-115
Preprint. Discussion started: 14 July 2020

Geoscientific Model Development Discussions
Open Access
EGU

Table 1. Data of four large earthquakes occurred in SUB3 and reported by Rodríguez-Pérez et al. (2018). Specifically, the date of occurrence; moment magnitude M_{w}; effective length L_{eff} and wide W_{eff} of the area following the methodology in Mai and Beroza (2000); asperity area A_{a}; and the epicentral coordinates Lon and Lat

Date	M_{w}	L_{eff} $[km]$	W_{eff} $[km]$	Z $[km]$	$S_{\mathrm{a}} = A_{\mathrm{a}}/A_{\mathrm{eff}}$	Lon Deg.	Lat Deg.	color*	SA region
14/09/1995	7.4	68.80	46.61	16	0.23	-98.76	16.48	green	1
25/02/1996	7.1	61.70	56.54	25	0.18	-98.25	15.83	red	2
19/07/1997	6.5	23.27	17.51	15	0.26	-98.35	15.86	orange	3
20/03/2012	7.4	54.94	53.59	19	0.26	-98.43	16.41	magenta	4

https://doi.org/10.5194/gmd-2020-115
Preprint. Discussion started: 14 July 2020

Geoscientific Model Development Discussions
Open Access
EGU

Table 2. Additional data of the sub-seismic regions: area and aspect ratio

sub-sesimic region	$Area$ $[km^2]$	Aspect ratio χ	color*
1	3206.77	1.48	green
2	3488.52	1.09	red
3	407.46	1.33	orange
4	2944.23	1.03	magenta

*color area in-Fig. 4.